Contents lists available at ScienceDirect

Chemical Engineering Research and Design

journal homepage: www.elsevier.com/locate/cherd

Structure-heat transport analysis of periodic open-cell foams to be used as catalyst carriers

Christoph Sinn[a], *Jonas Wentrup*[a], *Georg R. Pesch*[a,*], *Jorg Thöming*[a], *Lars Kiewidt*[b,*]

[a] *University of Bremen, Chemical Process Engineering, Leobener Strasse 6, 28359 Bremen, Germany*
[b] *Wageningen University & Research, Biobased Chemistry and Technology, P.O. Box 17, 6700 AA Wageningen, The Netherlands*

ARTICLE INFO

Article history:
Received 12 June 2020
Received in revised form 18 November 2020
Accepted 9 December 2020
Available online 17 December 2020

Keywords:
Open-cell foams
Kelvin cells
Conjugate heat transfer
CFD
Temperature distribution
Tailored design

ABSTRACT

Open-cell foams are promising catalyst supports as they provide a low pressure drop, radial mixing, and exceptional heat transport properties. Even though their large potential for the design of small-scale, dynamically operated reactors with strongly exothermic reactions is known, their application is not yet common. To design efficient and safe structured reactors in the future, the understanding of structure-heat transport relations is key. Fully resolved CFD simulations of non-isothermal structured reactors including chemical surface reactions require a high modeling effort and are computationally expensive. In a previous study we therefore implemented volumetrically distributed heat sources in the solid to mimic the heat production during an exothermal reaction, and evaluated the resulting heat flows and temperature distributions via CFD. The previous analysis, however, was limited to one specific open-cell foam geometry. In this study, we extend the conjugate heat transfer problem including heat production in the solid to five periodic open-cell foams (Kelvin cell-lattices) with defined but different structural parameters to establish structure-heat transport relations. We confirmed conduction being the dominant heat removal mechanism and found the strut diameter and the solid thermal conductivity being the key parameters to improve heat transport and reduce hot spots.

1. Introduction

Cellular and interconnected open-cell foam structures provide a remarkable potential for process intensification in, among others, solar receivers, pore burners, and catalytic reactors (Wu and Wang, 2013; Gao et al., 2014; Kiewidt and Thöming, 2019a). Their potential for intensification of exo- and endothermic catalytic reactions is based on their outstanding radial heat transport, high radial mixing, and low pressure loss (Bianchi et al., 2012; Gräf et al., 2014).

The thermal management during catalytic reactions is crucial in reactor design to obtain optimal temperature profiles (Kiewidt and Thöming, 2015) and to avoid hot-spot formation (Gräf et al., 2016). Although the use of open-cell foams in highly exothermic reactions, such as the CO_2-methanation in Power-to-Gas (PtG) applications, has been reported several times, they are not yet widely used in commercial applications (Montenegro Camacho et al., 2018; Kiewidt and Thöming, 2019b). A main reason is the difficult mounting with proper wall coupling, especially for large multi-tubular fixed-bed reactors (e.g., Haber-Bosch process, methane reforming) (Reitzmann et al., 2006). For small-scale dynamic reactors, which are needed in the future for Power-to-X (PtX) processes, however, open-cell foams provide resilient heat transport over

* *Corresponding authors.*
E-mail addresses: gpesch@uni-bremen.de (G.R. Pesch), lars.kiewidt@wur.nl (L. Kiewidt).
https://doi.org/10.1016/j.cherd.2020.12.007

Nomenclature

Roman

A_s	strut surface area, m^2
A_W	wall contact area of the solid, m^2
$c_{p,f}$	fluid isobaric heat capacity, J Kg^{-1} K^{-1}
$c_{p,s}$	solid isobaric heat capacity, J Kg^{-1} K^{-1}
C	coefficients for surrogate model
d_c	cell diameter, m
d_s	strut diameter, m
F	heat flow, W
F_{SW}	heat flow from solid to wall, W
F_{SF}	heat flow from solid to fluid, W
h	specific enthalpy, kJ
p	pressure, p
S	total heat source, W
S_{spec}	specific heat source, W m^{-3}
S_V	specific surface area, m^{-1}
T	temperature, K
T_s	solid temperature, K
T_f	fluid temperature, K
T_W	wall temperature, K
T_{max}	maximum solid temperature, K
u, U	velocity, m s^{-1}
V_s	solid volume, m^3
v	superficial velocity, m s^{-1}

Greek

α	heat transfer coefficient, W m^{-2} K^{-1}
ε_o	open porosity, -
μ	dynamic viscosity, Pa s
λ_f	fluid thermal conductivity, W m^{-1} K^{-1}
λ_s	solid thermal conductivity, W m^{-1} K^{-1}
ρ_f	fluid density, Kg m^{-3}
ρ_s	solid density, Kg m^{-3}
β	parameter of surrogate model, m^{-1}

Dimensionless groups

Re_p	pore Reynolds number, -

a wide range of flow rates due to dominant heat removal by thermal conduction in the solid phase (Kalz et al., 2017; Kiewidt and Thöming, 2019b).

Foam structured reactors, however, are only able to outperform conventional pellet fixed-bed reactors if conduction is the dominant heat removal mechanism (Kiewidt and Thöming, 2019b). The fractions of heat removal by thermal conduction, convective transport, and thermal radiation depend largely on the structure (strut diameter, cell and window diameter) of the open-cell foam (Bianchi et al., 2012; Wallenstein et al., 2014; Fischedick et al., 2017; Xu et al., 2019). To design small-scale structured reactors with robust heat transport and parametric stability, fundamental understanding and quantification of the relations between the structure of open-cell foams and the dominant mechanisms of heat removal is key. Although several studies already related a high effective two-phase thermal conductivity of open-cell foams to low porosities (high solid content) and high intrinsic material thermal conductivities (Fourie and Du Plessis, 2004; Edouard, 2011; Bianchi et al., 2012; Kumar and Topin, 2014; Wallenstein et al., 2014; Ranut, 2016; Fischedick et al., 2017), the contributions of different mechanisms to actual heat removal in open-cell foams with internal heat production have not been quantified yet.

In the past, full-field three-dimensional CFD simulations of open-cell foams proved to be valuable to get insight into different heat transport mechanisms in open-cell foams as they allow the computation of undisturbed (e.g. from experimental probes) temperature fields and heat flows of solid and fluid phases. CFD was successfully applied to study the influence of geometry, material, velocity, and wall coupling (Zafari et al., 2015; Torre et al., 2015; Bianchi et al., 2015; Razza et al., 2016). Despite their advantages, CFD simulations of full-field catalytic surface reactions in open-cell foams are challenging due to the high computational cost and modeling effort (Torre et al., 2016; Wehinger et al., 2016; Dong et al., 2018). Furthermore, CFD simulations usually provide results for only one specific foam structure and thus require the creation and meshing of several geometries to establish structure-transport relations. The geometries can be obtained through tomography (image-based Ranut et al., 2015; Sadeghi et al., 2020), through idealization (e.g., Kelvin cells and periodic open-cell foams (POCS), Torre et al., 2016; Iasiello et al., 2017; Lucci et al., 2017) or computer algorithms (i.e., Voronoi-tessellations, Bracconi et al., 2018; Wehinger et al., 2016). Generally, image-based CFD models preserve the original open-cell foam geometry accurately but are time consuming if several foam geometries need to be compared. Furthermore, geometrical properties of these reticulated foams are distributed and thus more difficult to characterize in comparison to regular structures. Hence, methods for the creation of artificial, regular open-cell foam geometries were mostly used to investigate structure-transport relations (Bracconi et al., 2018; Bianchi et al., 2016). These studies investigated the effect of the strut-to-node ratio on the effective thermal conductivity and found that the solid distribution along the strut and between strut and nodes is key for the overall foam's conduction properties. In another recent study, Bracconi et al. varied the solid content (i.e., the porosity) radially and axially along the foam lattice and found an increased effective solid thermal conductivity if more solid material (i.e., thicker struts) is aligned radially (Bracconi et al., 2020). Nevertheless, the influence of the strut and cell design of foams on temperature distributions and heat flows under coupled conductive and convective heat transport as well as heat production within the solid (for example through chemical reactions) has not been analyzed yet. These close-to-realistic conditions with gas flow and heat production within the solid (instead of heating through the wall or the fluid inlet) contribute to the better understanding and quantification of heat removal mechanisms, and thus enable the improved design of structured chemical reactors.

In a previous study, we analyzed conjugate heat transfer simulations including heat production within the solid to mimic an exothermic chemical reaction (Sinn et al., 2019). The procedure allows to investigate the effect of heat production on solid and fluid temperature fields as well as on heat flows while saving the modeling and solution effort of species transport and chemical surface reactions. In the previous study, we found inhomogeneous temperature fields in a solid ceramic foam due to the heat production in the solid. We concluded that solid temperature distributions in foams during exothermal reactions cannot generally be assumed as homogeneous for relevant process conditions in heterogeneous catalysis (heat sources from 5 to 150 W, e.g., for CO_2 methanation reaction, solid thermal conductivities from 5 to 50 W m^{-1} K^{-1}, i.e., ceramic foams, and superficial velocities from 0 to 0.5 m s^{-1}).

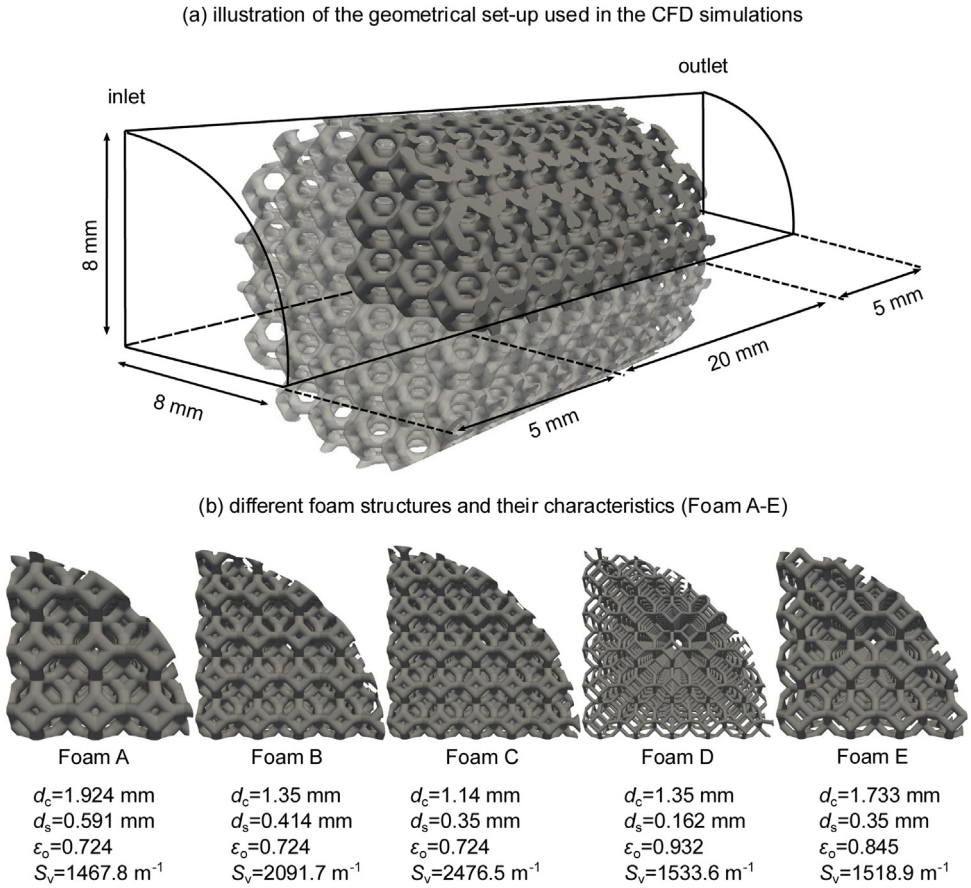

Fig. 1 – Geometries of the five periodic open-cell foams (Kelvin lattices) investigated in this study.

We also showed that homogeneous models cannot resolve the temperature inhomogeneities sufficiently so that detailed 3D simulations are necessary (Sinn et al., 2019; 2020). Further, we showed that the ratio between convective and conductive heat flows from the solid shifts from conduction-dominated to convection-dominated with increasing superficial velocities and decreasing solid thermal conductivities. The study thus demonstrated the potential of the approach to mimic exothermic chemical reactions by a distributed heat source in the solid domain. The present study expands the heat source approach to other open-cell foam geometries and conducts a structure-heat transport analysis for geometries, solid thermal conductivities, and fluid velocities relevant in heterogeneous catalysis.

Here, we investigate five different periodic open-cell foam geometries (POCS, Kelvin cell lattices) via CFD and correlate heat flows and temperature increases for heat production within the solid with the geometrical descriptors strut and cell diameter via a semi-empirical model. The novel contribution of this work is thus the quantification and modelling of the contributions of conductive and convective heat removal from open-cell foam structures with heat production in the solid, as it occurs in open-cell foams in structured catalytic fixed-bed reactors.

2. Methods

2.1. *Creation of foam geometries and setup of CFD model*

To establish structure-transport relations of the periodic open-cell foams, we adopted the same CFD model as described in our previous work (Sinn et al., 2019). The model describes a laminar steady-state conjugate heat transfer problem between flowing air and an open-cell foam (see Appendix A and Sinn et al., 2019). The model was established in the OpenFOAM® simulation framework (Version 5.0, Weller et al., 1998). The solid foam contained a uniformly distributed volumetric heat source that mimics the heat of reaction (called S). The model was verified against other CFD data from literature as well as against heat transfer and pressure drop correlations in a previous study (Sinn et al., 2019).

For this study, we chose five different Kelvin cell lattices (see Fig. 1). Due to their well-defined morphology, the Kelvin cell properties could be easily varied and examined according to their impact on fluid flow and thermal phenomena (Torre et al., 2014). Although, Kelvin cell lattices (or POCS) underperformed reticulated foams in terms of heat and mass transfer due to lower radial mixing (Horneber et al., 2012), recent studies showed the potential of idealized structures for process intensification (Bracconi et al., 2018). Especially the rise of additive manufacturing techniques facilitates using POCS to tailor catalyst supports (Zhou and Liu, 2017).

Kelvin cells are characterized by the four foam properties: cell diameter d_c, strut diameter d_s, open porosity ε_o and specific surface area S_v. Due to explicit dependencies, two of them are sufficient to define the overall structure (Inayat et al., 2011). The lattices were created using the CAD tool Autodesk Fusion 360, using the cell diameter d_c and the strut diameter d_s as input parameters. The open porosity ε_o and the specific surface area S_v were extracted from the final lattice geometries using the CAD software. The selected Kelvin

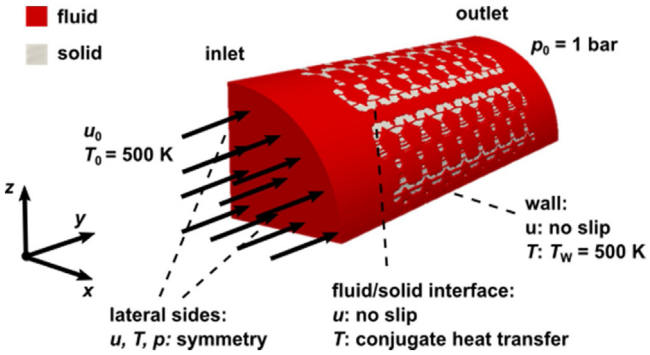

Fig. 2 – Illustration of the applied boundary conditions.

cell lattices have geometric properties that are relevant in heterogeneous catalysis and therefore are suitable for the investigation of heat production in different foam geometries. Additionally, the periodic Kelvin cell lattice allowed for accelerated computation by only simulating a quarter of the geometry. Grid independence studies were conducted to ensure mesh-independent results (see Appendix B).

2.2. *Boundary conditions*

This study extends the parameter range of the previous study (Sinn et al., 2019) by varying the geometry. Hence, the same process and boundary conditions as in our previous study were applied (Sinn et al., 2019). The only difference is caused by the choice of the quarter pipe system, which has two symmetry boundary conditions to account for the whole geometry (see Fig. 2). The initial temperature of the air flow was identical to the fixed wall temperature (500 K). Heat energy could thus only enter the system through the applied heat sources.

2.3. *Selection of structure descriptors*

The geometric foam properties (cell diameter d_c, strut diameter d_s, open porosity ε_o and specific surface area S_v) might not all be necessary to properly conduct a structure heat transport analysis. Therefore, the scatter plots shown in Fig. 3 indicate trends between the geometrical properties of the structures. Note that specific surface area and open porosity were determined from the created geometry and not from model equations. The trendlines and correlation coefficients were computed using conventional univariate linear regression. The specific surface area correlates negatively with the cell diameters (R^2 = 0.628, panel d), while the strut diameter correlates negatively with the open porosity (R^2 = 0.637, panel a). In contrast, neither cell diameter and open porosity (R^2 = 0.002, panel b) nor strut diameter and specific surface area (R^2 = 0.001, panel c) indicate any correlation for the investigated structures. The results thus suggest to choose the strut and cell diameter as principal geometric descriptors for the structure-transport analysis. Note that the data in Fig. 3 is not intended to derive general quantitative correlations of the structural parameters but highlights principal qualitative trends in the dependencies between the structural parameters, which are in line with existing semi-empirical correlations for the open porosity ε_o and the specific surface area S_v (Inayat et al., 2011; Lucci et al., 2014). For reticulated foams one would probably use the specific surface area and the open porosity as descriptors as these two parameters are easily determined experimentally.

3. Results and discussion

3.1. *Influence of heat sources on heat flows and temperature distributions*

The only thermal energy entering the system is caused by the volumetric heat source within the solid, the energy balance at steady state thus reads (Sinn et al., 2019):

$$S = F_{SW} + F_{SF} \rightarrow 1 = \frac{F_{SW}}{S} + \frac{F_{SF}}{S} \quad (1)$$

where S denotes heat source intensity, F_{SW} denotes the heat flow from solid to the wall (conducted heat flow) and F_{SF} denotes the heat flow from solid to the fluid phase (convective heat flow). The influence of the heat source intensity on the specific heat flow from the solid foam to the wall for Foam A is plotted against the superficial velocity v in Fig. 4a. A value lower than 0.5 (see dashed read line in Fig. 4a) indicates that convection is the dominant heat transport mechanism whereas a value above 0.5 indicates thermal conduction being dominant. By normalizing the conducted heat flow F_{SW} with the applied heat source intensity S, the data for the three investigated heat sources (5 W, 50 W and 150 W) collapsed for alumina (15 W m^{-1} K^{-1}) at every superficial velocity. The same behavior was observed for the 10 ppi foam in (Sinn et al., 2019) as well as for the structures B–E (not plotted here). The normalization indicates that the fraction of heat removed through thermal conduction or convection is independent of the intensity of the heat source. Furthermore, the general trend of a decreasing conductive heat transport (hence, increasing convective heat transport) for increasing superficial velocities was seen for all five geometries. Generally, the material with the highest thermal conductivity (sSiC, 50 W m^{-1} K^{-1}) showed the highest ratio of conducted heat flow to heat source intensity.

Next to the influence of heat sources on the heat flows, the influence on the temperature distribution in a foam has also been addressed. The approach revealed significant temperature inhomogeneities within the solid domain. Fig. 5 shows temperature fields for the investigated geometries with an applied 50 W heat source for a superficial velocity of 0.104 m s^{-1}. Here again, all foams and setups exhibited strong radial differences in the temperature field, which indicates that solid temperature fields in catalyst carriers based on ceramic foams can generally not be assumed as homogeneous. The position of the simulated hot-spots was in the rear part of the foam even though the axial temperature differences were comparably small. The axial temperature difference occured due to the cooling effect of the fluid when the flow entered the porous structure, while it is heated up already when reaching the rear part of the foam. Moreover, it became obvious that the temperature deviations from 500 K depend significantly on the structure (see Fig. 5). A severe maximum temperature increase was clearly seen for foams A–E. Moreover, for the given boundary conditions we observed a decreasing solid maximum temperature with increasing velocity (see Fig. 4b). This behavior was more pronounced for mullite than for alumina and sSiC. For the latter two materials, the decrease was only slight.

Similar to the specific heat flows, when the maximum temperature increase was normalized by the heat source intensities, ΔT_{max} S^{-1}, and plotted against superficial velocity, the points collapsed for identical solid thermal conductiv-

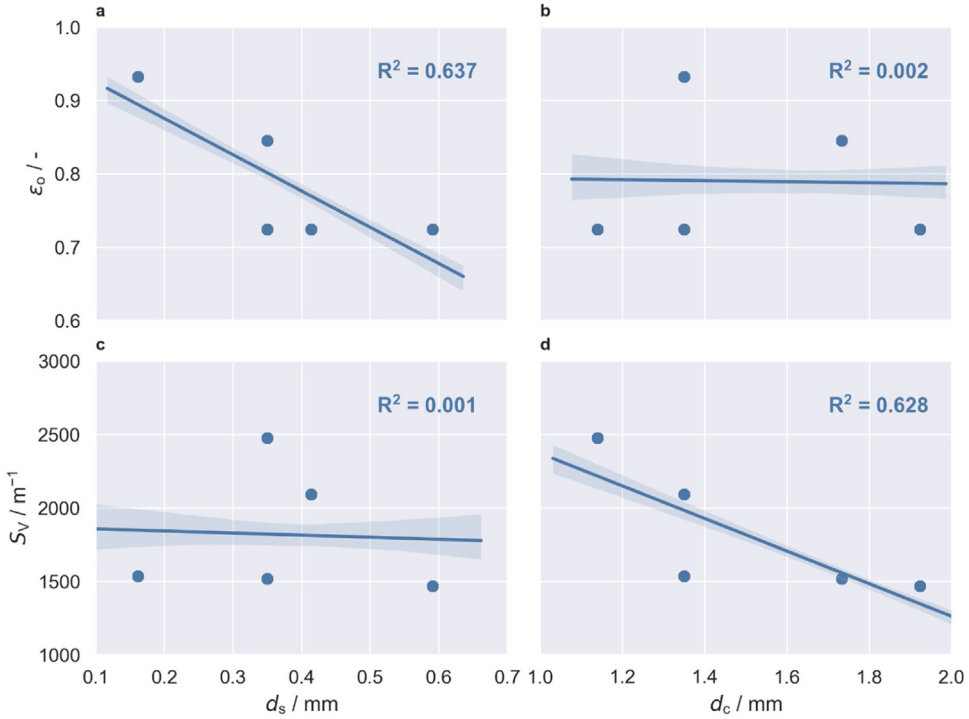

Fig. 3 – Analysis of the created foam geometries. Trends between strut diameter d_s and open porosity ε_o (a) as well as between cell diameter d_c and specific surface area S_V (d) can be observed. The shaded areas indicate 95% confidence intervals of the estimated slope. The strut diameter and cell diameters are thus used as structure descriptors. Note that both S_V and ε_o are determined from the created geometry and not from model equations.

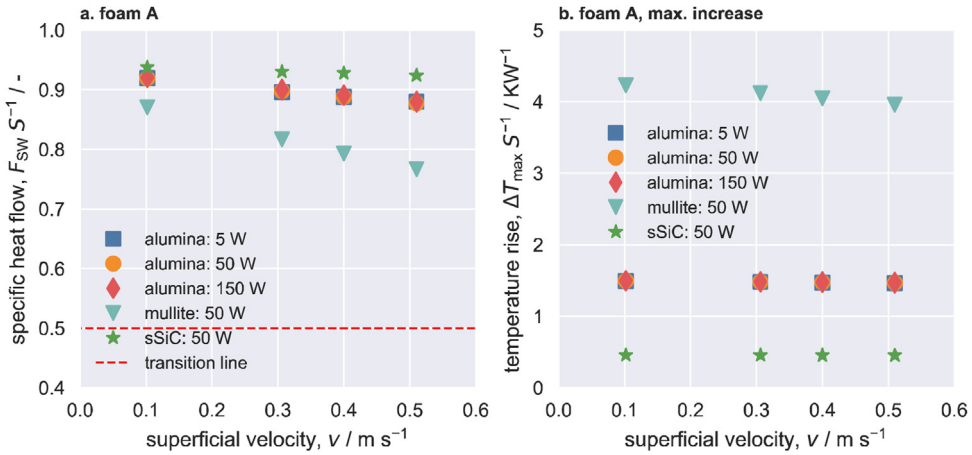

Fig. 4 – Thermal effects of heat sources on Foam A for different materials (i.e., thermal conductivities). a) Specific conductive heat flow F_{SW} S^{-1} plotted against the velocity v for different materials and heat sources; the transition line indicates the crossing from dominant convection (F_{SW} S^{-1} < 0.5) to dominant conduction (F_{SW} S^{-1} > 0.5). b) Specific temperature increase ΔT_{max} S^{-1} (from initial 500 K) against the superficial velocity v.

ity (Fig. 4b). That means, that regardless of the heat source intensity between 5 W and 150 W, the maximum temperature increase can be estimated. Furthermore, the trends of maximum and mean temperature increases behave similarly and indicate that the entire temperature distribution shifts consistently (see Fig. 5). This behavior was also reported in the previous study (Sinn et al., 2019). When comparing the materials, all relations between temperature increase and superficial velocity show linear behavior regardless of the structure or material. For the μCT foam sample from the previous publication, mullite had an asymptotic trend, indicating heat transport limitations of the material and corresponding setup.

3.2. *Influence of structure parameters on heat flows and temperature distributions*

So far, the results for the 10 ppi foam found in Sinn et al. (2019) were also observed for the different periodic open-cell foams in this study. Severe differences in the temperature fields caused by the different geometries became apparent (see Fig. 5). To understand the relation between the foams' structure and their heat transport properties, we analyzed results from 100 simulations with unique combinations of strut and cell diameter, solid thermal conductivity, and fluid velocity. The specific conductive heat flows and maximum temperature increases, both normalized by the heat source

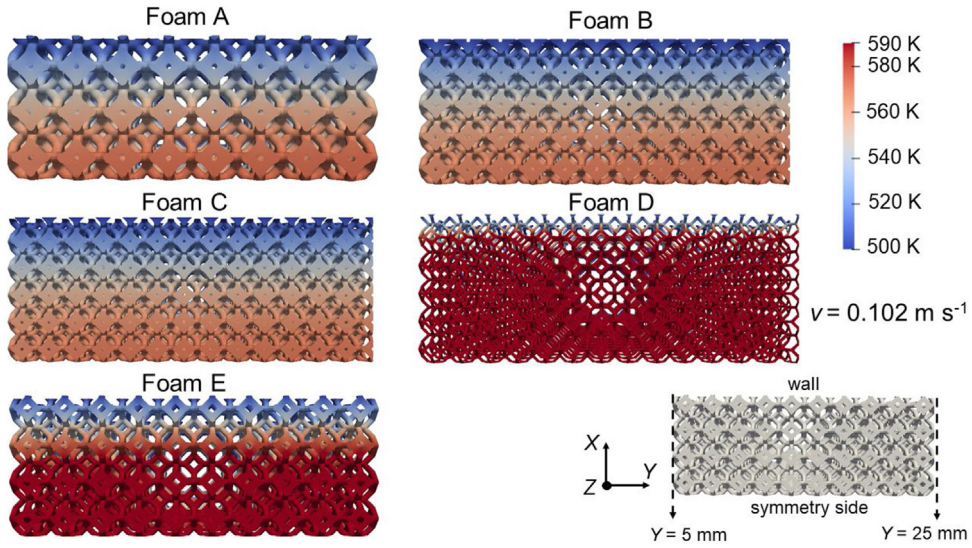

Fig. 5 – Temperature fields in the center plane for a 50 W heat source, a thermal conductivity of 15 W m^{-1} K^{-1} (i.e., alumina) and superficial velocity of 0.102 m s^{-1} for Foams A–E. Note that for clarity the temperature scale is limited to 590 K.

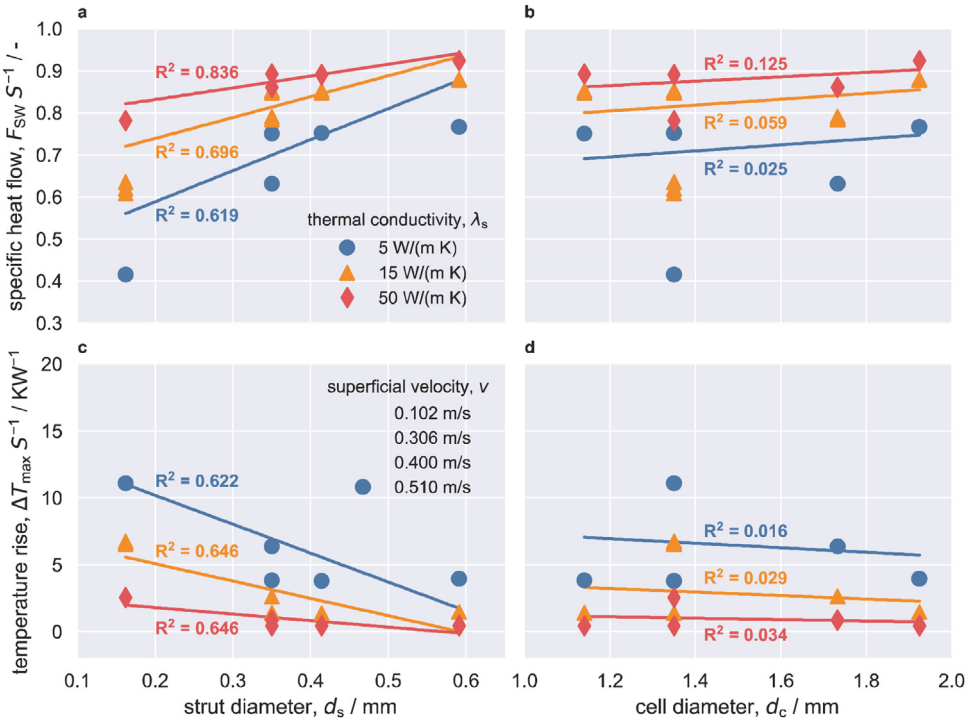

Fig. 6 – Relations between strut and cell diameter and specific heat flows (a and b) as well as specific maximal temperature increase (c and d). In total, results from 100 simulations of unique combinations of the strut and cell diameter, solid thermal conductivity, and fluid velocity were included. Different symbols and colors encode different solid thermal conductivities; different color shades indicate different fluid velocities. The trendlines and coefficients of determination (R^2) were determined using linear regression for the sets of different solid thermal conductivities.

intensity, were plotted against the strut and cell diameter (the chosen geometrical descriptors) in Fig. 6.

The specific conductive heat flows for almost all investigated cell and strut diameters were above 0.5 indicating dominant conduction (panels a and b). Only the smallest strut diameter (0.162 mm, Foam D) alongside with the lowest solid thermal conductivity (5 W m^{-1} K^{-1}) showed specific heat flows below 0.5 and thus dominant heat removal through convection (see Fig. 6a). The reason certainly is the small strut diameter which hinders conductive heat transport through the solid struts. This is in accordance with the findings of Zafari et al. (2015) and Bracconi et al. (2018).

Fig. 6a also clearly shows that an increasing strut diameter shifts the conduction/convection ratio significantly to conduction. The structure with the highest conduction ratio is thus the one with the largest strut diameter (d_s = 0.591 mm). The strong influence of the strut diameter is also reflected in the coefficients of determination (R^2) of the fitted linear trendlines. The coefficients of determination decrease from 0.836 over 0.696 to 0.619 with decreasing solid thermal conductivity indicating a significant relation between the strut diameter and the specific conductive heat flows. The strength of the correlation between the strut diameter and the specific conductive heat flow decreases for lower solid thermal

conductivities due the increasing influence of conductive heat removal. In contrast, the highest coefficient of determination between the cell diameter and the specific heat flow is 0.125 (Fig. 6b). The cell diameter does thus not influence the specific heat flow.

Inversely to the specific heat flow, the specific temperature increase (from the initial 500 K) decreased with increasing strut diameter and thermal conductivity (Fig. 6c). Again, the strut diameter significantly determines the observed temperature rise as indicated by the coefficients of determination around 0.6 for all solid thermal conductivities. In contrast, to the heat flows, the coefficients of determination did not change with the solid thermal conductivity. Again, the obtained coefficients of determination between the cell diameter and the specific temperature increase were below 0.1 (Fig. 6d), confirming the observation that the cell diameter does not determine the heat transport in the investigated parameter space.

3.3. *Quantitative analysis of structure-transport relations*

The previous exploratory analysis showed that the strut diameter d_s, the solid thermal conductivity λ_s, and the fluid velocity v are the principal structure and process parameters that determine heat flows in POCS with heat generation. To quantify the described structure-transport relations, we developed a simple yet physically sound surrogate model that describes the heat flows in the investigated system (see Fig. 7). The model consists of a cylindrical strut representing the periodic open-cellular structure. The strut reaches from the center of the tube at $y = 0$ to the wall at $y = C_L$. C_L is a characteristic length that describes the pathway for thermal conduction within the strut. Along the strut, energy is transferred to the surrounding fluid by convection. As in the CFD model, energy is produced within the strut. At the center of the strut ($y = 0$), a symmetry boundary condition is applied. At the wall ($y = C_L$), a fixed temperature equal to the incoming fluid temperature is assumed as for the CFD model. The steady state energy balance and boundary conditions for the strut thus read

$$\lambda_s \frac{d^2T_s}{dy^2} = \frac{A_s}{V_S}\alpha\,(T_s - T_f) - \frac{S}{V_S} \text{ subject to } \left.\frac{dT_s}{dy}\right|_{y=0} = 0 \text{ and } T_s\,(y = C_L) = T_f \quad (2)$$

The differential Eq. (2) is solved analytically using Matlab's Symbolic Math Toolbox (The MathWorks, 2019). Afterwards, the conductive heat flow is calculated from the temperature gradient at the wall ($y = C_L$). The resulting expression for the normalized conductive heat flow is

$$\frac{F_{SW}}{S} = \frac{C_A}{\sqrt{C_S}\,\beta}\tanh\left(\sqrt{C_S}\,C_L\,\beta\right) \text{ . with } \beta = \sqrt{\frac{\alpha}{d_s\lambda_s}} \quad (3)$$

As previously explained, the parameter C_L describes the pathway of heat conduction within the solid. The parameter C_s describes the shape of the strut so that

$$\frac{A_s}{V_s} = \frac{C_s}{d_s} \quad (4)$$

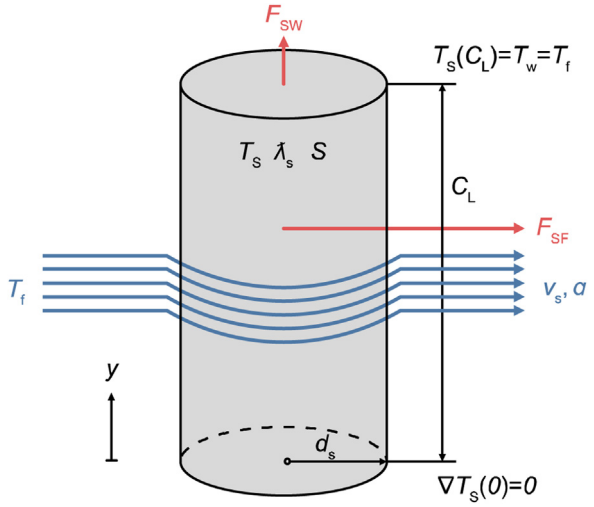

Fig. 7 – Illustration of the surrogate structure-transport model.

Table 1 – Summary of the setup and results of the non-linear least-squares minimization.

Quantity	Initial value	Final value
C_A (in m^{-1})	657.8	486.1 ± 8.7 (1.80%)
C_L (in mm)	21.85	1.91 ± 0.04 (2.19%)
C_s	4 (fixed)	4 (fixed)
correlation coeff. (C_A, C_L)		−0.98
number of data points		100
number of parameters		2
reduced SSE		$7.415\ 10^{-4}$

For the cylindrical struts in this study, C_s was set to 4. The parameter

$$C_A = \frac{A_w}{V_s} \quad (5)$$

describes the ratio of the wall contact area of the solid A_W and the solid volume V_s.

The heat transfer coefficient α depends on the strut diameter d_s and the fluid velocity v. For the present study, the heat transfer coefficient was estimated from Gnielinski's expression for laminar flow over a single cylinder (Martin and Gnielinski, 2000).

The influence of the principal parameters (strut diameter, solid thermal conductivity, and fluid velocity) is thus captured in the single parameter β in Eq. (3). The remaining unknown parameters are C_A and C_L. Both parameters were determined from the CFD data using non-linear least-squares minimization. To avoid local minima, 1000 random combinations from the parameter space $C_A \in 0\,m^{-1}, 1000\,m^{-1}$ and $C_L \in 0\,m, 1\,m$) were sampled, and the combination with the lowest sum of square errors (SSE) was selected.

Table 1 shows the setup and summary of the non-linear least-squares minimization. For both parameters, C_A and C_L, the standard deviation of the estimated values is below 5%, however, both parameters are strongly negatively correlated. The strong correlation is reasonable from a physical perspective as both parameters describe geometric features of the solid structure, and thus depend on the geometric structure parameters. Nevertheless, the developed structure-transport model describes the CFD data with an overall accuracy of ±10% (see Fig. 8). The deviations increase for small strut diameters and high fluid velocities, for which complex flow patterns

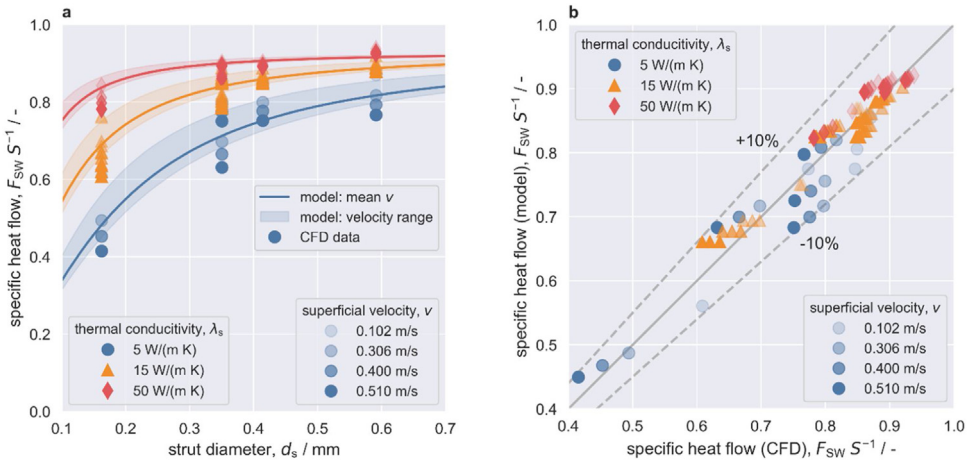

Fig. 8 – Comparison of model predictions with the CFD data (a), and parity plot of specific heat flow calculated with the structure-transport model and the CFD model (b). The structure-transport model predicts the CFD data within ±10% accuracy. The solid lines in (a) were calculated with the mean of the investigated velocity (0.31 m s^{-1}); the shaded areas represent the velocity range in the structure-transport model.[2]

increase the influence of the convective heat transfer. The complexity of the flow patterns is not fully captured in the surrogate structure-transport model.

Overall, the developed structure-transport model provides a valuable tool to quickly estimate the contributions of different heat transport mechanisms in POCS with heat generation in the solid, and will thus facilitate the design of tailored structured catalyst carriers in the future. Furthermore, the physical basis of the structure-transport model allows its extension to other structures such as irregular open-cell foams.

4. Conclusion

The conducted structure-heat transport analysis shows that the strut diameter and the thermal conductivity are the dominant structural parameters to control heat removal in periodic open-cell foams for typical materials and conditions found in gas-phase heterogeneous catalysis. The cell diameter, in contrast, does not influence heat removal. The fluid velocity plays a significant role only for materials with a low solid thermal conductivity. The high influence of the strut diameter and the thermal conductivity underpins the impact of thermal conduction in the solid domain. Due to the close resemblance of the Kelvin unit cell with the cells found in regular open-cell foams, the results obtained in this study for periodic open-cell foams (Kelvin lattices) are likely to translate well to regular open-cell foams. The found structure-heat transport relations thus underline the potential of open-cell foams (periodic and regular) to decouple effective heat removal from the fluid velocity in the design of catalyst carriers. In contrast to packed beds with point contacts between the individual catalyst particles, the decoupling trough structured catalyst carriers allows to use low flow rates in fixed-bed reactors, which leads to lower pressure drops and shorter reactors, while heat removal is guaranteed through the structure. In this case, sufficient mass transfer from the gas to the solid phase is the only constraint on the fluid velocity, which is typically less severe than for heat transfer.

Declaration of Competing Interest

The authors report no declarations of interest.

Acknowledgments

Christoph Sinn and Jorg Thöming appreciate the funding by the German Research Foundation (DFG) through the priority program SPP 2080 (Katalysatoren und Reaktoren unter dynamischen Betriebsbedingungen für die Energiespeicherung und -wandlung) under grant TH 893/23-1.

Appendix A. Governing equations and model assumptions (similar to (Sinn et al., 2019))

For the Newtonian fluid (air) with neglected gravitation, the conservation equations for mass, momentum, and energy as well as the ideal gas law read

$$\nabla \cdot (\rho_f \mathbf{U}) = 0, \quad (6)$$

$$\nabla \cdot (\rho_f \mathbf{U} \otimes \mathbf{U}) + \nabla \cdot (\mu(\nabla \otimes \mathbf{U} + (\nabla \otimes \mathbf{U})^T) - 2/3\mu(\nabla \cdot \mathbf{U})\mathbf{I}) - \nabla p = 0, \quad (7)$$

$$-\nabla \cdot (\rho_f \mathbf{U} h) - \nabla \cdot (\lambda_f \nabla T_f) = 0, \quad (8)$$

with ρ_f denoting fluid's density, $\mathbf{U}$ denoting the velocity field, h denoting the enthalpy and λ_f the fluid's thermal conductivity. In contrast, the solid phase is described by only the conservation of energy

$$\lambda_s(\nabla^2 T_s) + S_{spec} = 0, \quad (9)$$

with λ_s being the solid's thermal conductivity, T_s the solid's temperature and S_{spec} the specific artificial heat source. The simulations were carried out using the OpenFOAM solver chtMultiRegionSimpleFoam.

Table A1.

[2] The dataset from this plot is openly available under Sinn, C. (Christoph); Wentrup, J. (Jonas); Kiewidt, L.W. (Lars) (2020): Structure-heat transport data of periodic open-cell foams. 4TU.ResearchData. Dataset. https://doi.org/10.4121/uuid:58531fa2-067b-4a81-a577-75594df891c3.

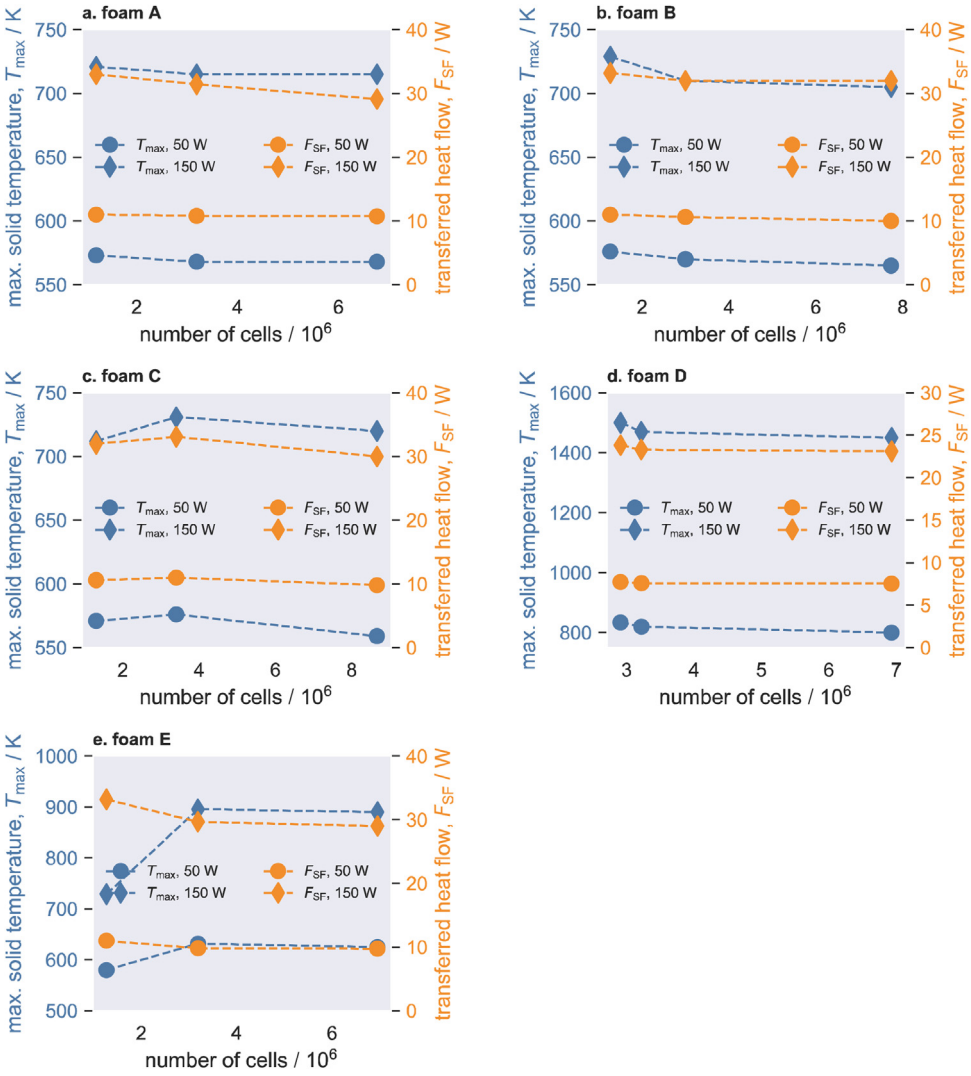

Fig. A1 – Grid independence studies for Foams A–E (λ_s = 15 W m^{-1} K^{-1}, v = 0.51 m s^{-1}). In all cases, the medium sized mesh has been selected.

Table A1 – Model properties investigated in this study.

Property		Assumption
Fluid dynamic viscosity	μ_f	Sutherland equation
Fluid heat capacity	$c_{p,f}$	const. (1030 J kg^{-1} K^{-1})
Fluid thermal conductivity	λ_f	Eucken approximation
Fluid density	ρ_f	ideal gas law (500 K: 0.7 Kg m−3)
Superficial velocity	v	const. (0.1–0.5 m s−1)
Pore Reynolds number	$Re_p = \frac{\rho_f v d_s}{\mu_f}$	const. (0.5–8)
Solid heat capacity	$c_{p,s}$	const. (1000 J kg^{-1} K^{-1}).
Solid thermal conductivity	λ_s	const. (5, 15 and 50 W m^{-1} K^{-1}) (alumina, mullite, sSiC)
Solid density	ρ_s	const. (4000 kg m^{-3})
Gravitational acceleration		neglected
Radiation		neglected
Turbulence		neglected

Appendix B. Grid independence studies

All meshes were created using the meshing utility snappyHexMesh. For further information regarding the meshing procedure the reader is referred to (Sinn et al., 2019).

Fig. A1

References

Bianchi, Enrico, Heidig, Tobias, Visconti, Carlo Giorgio, Groppi, Gianpiero, Freund, Hannsjorg, Tronconi, Enrico, 2012. An appraisal of the heat transfer properties of metallic open-cell foams for strongly exo-/Endo-Thermic catalytic processes in tubular reactors. Chem. Eng. J. 198–199, 512–528, http://dx.doi.org/10.1016/j.cej.2012.05.045.

Bianchi, Enrico, Groppi, Gianpiero, Schwieger, Wilhelm, Tronconi, Enrico, Freund, Hannsjörg, 2015. Numerical simulation of heat transfer in the near-wall region of tubular reactors packed with metal open-cell foams. Chem. Eng. J. 264, 268–279, http://dx.doi.org/10.1016/j.cej.2014.11.055.

Bianchi, Enrico, Schwieger, Wilhelm, Freund, Hannsjörg, 2016. Assessment of periodic open cellular structures for enhanced heat conduction in catalytic fixed-bed reactors. Adv. Eng. Mater. 18 (4), 608–614, http://dx.doi.org/10.1002/adem.201500356.

Bracconi, Mauro, Ambrosetti, Matteo, Maestri, Matteo, Groppi, Gianpiero, Tronconi, Enrico, 2018. A fundamental analysis of the influence of the geometrical properties on the effective thermal conductivity of open-cell foams. Chem. Eng. Process. Process. Intensif. 129 (July), 181–189, http://dx.doi.org/10.1016/j.cep.2018.04.018.

Bracconi, Mauro, Ambrosetti, Matteo, Maestri, Matteo, Groppi, Gianpiero, Tronconi, Enrico, 2020. Analysis of the effective

thermal conductivity of isotropic and anisotropic periodic open cellular structures for the intensification of catalytic processes. Chem. Eng. Process. Process. Intensif., 108169, http://dx.doi.org/10.1016/j.cep.2020.108169.

Dong, Ying, Korup, Oliver, Gerdts, Julian, Cuenya, Beatriz Roldán, Horn, Raimund, 2018. Microtomography-based CFD modeling of a fixed-bed reactor with an open-cell foam monolith and experimental verification by reactor profile measurements. Chem. Eng. J. 353, 176–188, http://dx.doi.org/10.1016/j.cej.2018.07.075.

Edouard, David, 2011. The effective thermal conductivity for 'slim' and 'fat' foams. AIChE J. 57 (6), 1646–1651, http://dx.doi.org/10.1002/aic.12372.

Fischedick, T., Kind, M., Dietrich, B., 2017. Radial two-phase thermal conductivity of ceramic sponges up to high temperatures – experimental results and correlation. Int. J. Therm. Sci. 114, 98–113, http://dx.doi.org/10.1016/j.ijthermalsci.2016.11.020.

Fourie, J.G., Du Plessis, J.P., 2004. Effective and coupled thermal conductivities of isotropic open-cellular foams. AIChE J. 50 (3), 547–556, http://dx.doi.org/10.1002/aic.10049.

Gao, H.B., Qu, Z.G., Feng, X.B., Tao, W.Q., 2014. Methane/air premixed combustion in a two-layer porous burner with different foam materials. Fuel 115, 154–161, http://dx.doi.org/10.1016/j.fuel.2013.06.023.

Gräf, Ingo, Rühl, Anne Kathrin, Kraushaar-Czarnetzki, Bettina, 2014. Experimental study of heat transport in catalytic sponge packings by monitoring spatial temperature profiles in a cooled-wall reactor. Chem. Eng. J. 244, 234–242, http://dx.doi.org/10.1016/j.cej.2014.01.060.

Gräf, Ingo, Ladenburger, Georg, Kraushaar-Czarnetzki, Bettina, 2016. Heat transport in catalytic sponge packings in the presence of an exothermal reaction: characterization by 2D modeling of experiments. Chem. Eng. J. 287, 425–435, http://dx.doi.org/10.1016/j.cej.2015.11.042.

Horneber, T., Rauh, C., Delgado, A., 2012. Fluid dynamic characterisation of porous solids in catalytic fixed-bed reactors. Microporous Mesoporous Mater. 154, 170–174, http://dx.doi.org/10.1016/j.micromeso.2011.12.047.

Iasiello, M., Cunsolo, S., Bianco, N., Chiu, W.K.S., Naso, V., 2017. Developing thermal flow in open-cell foams. Int. J. Therm. Sci. 111, 129–137, http://dx.doi.org/10.1016/j.ijthermalsci.2016.08.013.

Inayat, Amer, Freund, Hannsjörg, Zeiser, Thomas, Schwieger, Wilhelm, 2011. determining the specific surface area of ceramic foams: the tetrakaidecahedra model revisited. Chem. Eng. Sci. 66 (6), 1179–1188, http://dx.doi.org/10.1016/j.ces.2010.12.031.

Kalz, Kai F., Kraehnert, Ralph, Dvoyashkin, Muslim, Dittmeyer, Roland, Gläser, Roger, Krewer, Ulrike, Reuter, Karsten, Grunwaldt, Jan Dierk, 2017. Future challenges in heterogeneous catalysis: understanding catalysts under dynamic reaction conditions. ChemCatChem 9 (1), 17–29, http://dx.doi.org/10.1002/cctc.201600996.

Kiewidt, Lars, Thöming, Jorg, 2015. predicting optimal temperature profiles in single-stage fixed-bed reactors for CO_2-methanation. Chem. Eng. Sci. 132, 59–71, http://dx.doi.org/10.1016/j.ces.2015.03.068.

Kiewidt, Lars, Thöming, Jorg, 2019a. Multiscale modelling of monolithic sponges as catalyst carrier for the methanation of carbon dioxide. Chem. Eng. Sci.: X 2, 100016, http://dx.doi.org/10.1016/j.cesx.2019.100016.

Kiewidt, Lars, Thöming, Jorg, 2019b. Pareto-optimal design and assessment of monolithic sponges as catalyst carriers for exothermic reactions. Chem. Eng. J. 359, 496–504, http://dx.doi.org/10.1016/j.cej.2018.11.109.

Kumar, Prashant, Topin, Frederic, 2014. The geometric and thermohydraulic characterization of ceramic foams: an analytical approach. Acta Mater. 75, 273–286, http://dx.doi.org/10.1016/j.actamat.2014.04.061.

Lucci, Francesco, Torre, Augusto Della, Rickenbach, Janvon, Montenegro, Gianluca, Poulikakos, Dimos, Eggenschwiler, Panayotis Dimopoulos, 2014. Performance of randomized Kelvin cell structures as catalytic substrates: mass-transfer based analysis. Chem. Eng. Sci. 112, 143–151, http://dx.doi.org/10.1016/j.ces.2014.03.023.

Lucci, Francesco, Torre, Augusto Della, Montenegro, Gianluca, Kaufmann, Rolf, Eggenschwiler, Panayotis Dimopoulos, 2017. Comparison of geometrical, momentum and mass transfer characteristics of real foams to Kelvin cell lattices for catalyst applications. Int. J. Heat Mass Transf. 108, 341–350, http://dx.doi.org/10.1016/j.ijheatmasstransfer.2016.11.073.

Martin, Holger, Gnielinski, Volker, 2000. Calculation of heat transfer from pressure drop in tube bundles. The 3rd European Thermal Sciences Conference, 1155–1160.

Montenegro Camacho, Y.S., Bensaid, S., Lorentzou, S., Vlachos, N., Pantoleontos, G., Konstandopoulos, A., Luneau, M., et al., 2018. Development of a robust and efficient biogas processor for hydrogen production. Part 2: experimental campaign. Int. J. Hydrogen Energy 43 (1), 161–177, http://dx.doi.org/10.1016/j.ijhydene.2017.10.177.

Ranut, Paola, 2016. On the effective thermal conductivity of aluminum metal foams: review and improvement of the available empirical and analytical models. Appl. Therm. Eng. 101 (May), 496–524, http://dx.doi.org/10.1016/j.applthermaleng.2015.09.094.

Ranut, Paola, Nobile, Enrico, Mancini, Lucia, 2015. High resolution X-ray microtomography-based CFD simulation for the characterization of flow permeability and effective thermal conductivity of aluminum metal foams. Exp. Therm. Fluid Sci. 67, 30–36, http://dx.doi.org/10.1016/j.expthermflusci.2014.10.018.

Razza, S., Heidig, T., Bianchi, E., Groppi, G., Schwieger, W., Tronconi, E., Freund, H., 2016. heat transfer performance of structured catalytic reactors packed with metal foam supports: influence of wall coupling. Catal. Today 273, 187–195, http://dx.doi.org/10.1016/j.cattod.2016.02.058.

Reitzmann, Andreas, Patcas, Florina Corina, Kraushaar-Czarnetzki, Bettina, 2006. Keramische schwämme - anwendungspotenzial monolithischer netzstrukturen als katalytische packungen. ChemieIngenieurTechnik, http://dx.doi.org/10.1002/cite.200600029, WILEY-VCH Verlag.

Sadeghi, Mehrdad, Mirdrikvand, Mojtaba, Pesch, Georg R., Dreher, Wolfgang, Thöming, Jorg, 2020. Full-field analysis of gas flow within open-cell foams: comparison of micro-computed tomography-based CFD simulations with experimental magnetic resonance flow mapping data. Exp. Fluids 61 (5), 124, http://dx.doi.org/10.1007/s00348-020-02960-4.

Sinn, Christoph, Pesch, Georg R., Thöming, Jorg, Kiewidt, Lars, 2019. Coupled conjugate heat transfer and heat production in open-cell ceramic foams investigated using CFD. Int. J. Heat Mass Transf. 139, 600–612, http://dx.doi.org/10.1016/j.ijheatmasstransfer.2019.05.042.

Sinn, Christoph, Kranz, Felix, Wentrup, Jonas, Thöming, Jorg, Wehinger, Gregor D., Pesch, Georg R., 2020. CFD simulations of radiative heat transport in open-cell foam catalytic reactors. Catalysts 10 (6), 716, http://dx.doi.org/10.3390/catal10060716.

The MathWorks, 2019 2019. Symbolic Math Toolbox. Natick, Massachusetts, United States https://de.mathworks.com/help/symbolic/.

Torre, A., Della, G., Montenegro, G.R. Tabor, Wears, M.L., 2014. CFD characterization of flow regimes inside open cell foam substrates. Int. J. Heat Fluid Flow 50, 72–82, http://dx.doi.org/10.1016/j.ijheatfluidflow.2014.05.005.

Torre, A. Della, Montenegro, G., Onorati, A., Tabor, G., 2015. CFD characterization of pressure drop and heat transfer inside porous substrates. Energy Procedia 81, 836–845, http://dx.doi.org/10.1016/j.egypro.2015.12.093.

Torre, A. Della, Lucci, F., Montenegro, G., Onorati, A., Dimopoulos Eggenschwiler, P., Tronconi, E., Groppi, G., 2016. CFD modeling of catalytic reactions in open-cell foam substrates. Comput. Chem. Eng. 92, 55–63, http://dx.doi.org/10.1016/j.compchemeng.2016.04.031.

Wallenstein, M., Kind, M., Dietrich, B., 2014. Radial two-phase thermal conductivity and wall heat transfer coefficient of ceramic sponges – experimental results and correlation. Int. J.

Heat Mass Transf. 70, 486–495, http://dx.doi.org/10.1016/j.ijheatmasstransfer.2014.08.003.
Wehinger, Gregor D., Heitmann, Helge, Kraume, Matthias, 2016. An artificial structure modeler for 3D CFD simulations of catalytic foams. Chem. Eng. J. 284, 543–556, http://dx.doi.org/10.1016/j.cej.2015.09.014.
Weller, H.G., Tabor, G., Jasak, H., Fureby, C., 1998. A tensorial approach to computational continuum mechanics using object-oriented techniques. Comput. Phys. 12 (6), 620, http://dx.doi.org/10.1063/1.168744.
Wu, Zhiyong, Wang, Zhifeng, 2013. Fully coupled transient modeling of ceramic foam volumetric solar air receiver. Sol. Energy 89, 122–133, http://dx.doi.org/10.1016/j.solener.2012.12.016.
Xu, H.J., Xing, Z.B., Wang, F.Q., Cheng, Z.M., 2019. Review on heat conduction, heat convection, thermal radiation and phase change heat transfer of nanofluids in porous media: fundamentals and applications. Chem. Eng. Sci. 195, 462–483, http://dx.doi.org/10.1016/j.ces.2018.09.045.
Zafari, Mohammad, Panjepour, Masoud, Emami, Mohsen Davazdah, Meratian, Mahmood, 2015. Microtomography-based numerical simulation of fluid flow and heat transfer in open cell metal foams. Appl. Therm. Eng. 80, 347–354, http://dx.doi.org/10.1016/j.applthermaleng.2015.01.045.
Zhou, Xintong, Liu, Chang Jun, 2017. Three-dimensional printing for catalytic applications: current status and perspectives. Adv. Funct. Mater. 27 (30), 1701134, http://dx.doi.org/10.1002/adfm.201701134.